Intercalation induced ferromagnetism in group-V transition metal dichalcogenide bilayer

H. M. R. Ahamd, and Jian Zhou

COLLECTIONS

Paper published as part of the special topic on Chemical Physics, Energy, Fluids and Plasmas, Materials Science and Mathematical Physics

View Online   Export Citation   CrossMark

ARTICLES YOU MAY BE INTERESTED IN

Two-dimensional van der Waals spinterfaces and magnetic-interfaces
Applied Physics Reviews **7**, 011303 (2020); https://doi.org/10.1063/1.5112171

Two-dimensional multiferroic semiconductors with coexisting ferroelectricity and ferromagnetism
Applied Physics Letters **113**, 043102 (2018); https://doi.org/10.1063/1.5038037

The magnetic, electronic, and light-induced topological properties in two-dimensional hexagonal FeX_2 (X=Cl, Br, I) monolayers
Applied Physics Letters **116**, 192404 (2020); https://doi.org/10.1063/5.0006446

AIP Advances

AIP Publishing

Intercalation induced ferromagnetism in group-V transition metal dichalcogenide bilayer

H. M. R. Ahamd and Jian Zhou[a] (iD)

AFFILIATIONS

State Key Laboratory for Mechanical Behavior of Materials, Center for Advancing Materials Performance from the Nanoscale, Xi'an Jiaotong University, Xi'an 710049, China

[a]Author to whom correspondence should be addressed: jianzhou@xjtu.edu.cn

ABSTRACT

Two-dimensional (2D) ferromagnetic materials are receiving great attention in recent years. However, owing to strong direct magnetic coupling between different layers, they usually prefer antiferromagnetic coupling between different layers once stacked together. It would be of great interest if one can tune such antiferromagnetism to ferromagnetism, which is preferable for further magnetic information storage, and large magnetic moments can be achieved (proportional to thin-film thickness). In the current work, we theoretically and computationally suggest an effective method to tune the interlayer magnetic coupling between two magnetic materials (VX_2, X = S, and Se). We show that intercalating a layer of alkali metals could enhance indirect magnetic exchange, and ferromagnetic interlayer coupling between different VX_2 layers can be achieved. Our work provides a new and effective route to control and modulate the magnetic exchange between 2D magnetic materials.

INTRODUCTION

van der Waals stacked two-dimensional (2D) materials, owing to their rich and promising physical properties and potential applications, have been attracting great attention over the past few decades.[1] For example, when two layers of graphene sheets are stacked together, they could possess many different promising electronic behaviors, which can be further tuned by applying an external electric field,[2] stacking order,[3] and atomic intercalation.[4] Owing to the experimental advances of fabricating ultrathin 2D ferromagnetic (FM) monolayers, such as CrI_3,[5–8] $Cr_2Ge_2Te_6$,[9] and VSe_2,[10,11] these van der Waals stacked magnetic materials also promise to serve as potential magnetic memory and magnetic storage materials for magnetic random access memory (MRAM) devices in the near future. Unfortunately, even though a CrI_3 monolayer is ferromagnetic[5] (with its Curie temperature of 45 K), when two layers of CrI_3 are stacked together, they prefer antiferromagnetic (AFM) coupling at its ground state. Similar magnetic extinction also occurs in other systems. In order to tune their interlayer coupling into ferromagnetic, one could apply mechanical shear stress[12] or electrical gate voltage.[13]

Another interesting ferromagnetic (FM) material that has been recently discovered is group-V transition metal dichalcogenide (TMD) monolayer (for example VSe_2) with a high Curie temperature.[10] Compared with group-VI TMD monolayers (such as MoS_2 and its analogous structures), which are nonmagnetic,[14] the transition metals in group-V TMD are in their nd^1 (n = 3 or 4) electronic character. This unpaired electron makes the VSe_2 monolayer become spin-polarized, and the coupling between different V atoms prefers to be FM. Previous studies on these group-V TMD monolayers have suggested several interesting properties.[14–22] In 2012, Ma et al. performed density functional theory (DFT) calculations and predicted a strong ferromagnetic order of VS_2 monolayer,[23] which can be effectively tuned by a biaxial tensile strain. Owing to the breaking of time-reversal symmetry, Tong et al. predicted that the valley splitting of VSe_2 is not degenerate, which is coined as a novel concept, ferro-valley effect.[24] Larger valley degeneracy splitting with a time-reversal symmetry broken[25,26] is also predicted in heavier elements with strong valley polarized plasmonic behavior.[27]

With these promising properties of ferromagnetic group-V TMD *monolayers*,[14–16,18,21–23,28] when two layers are stacked

together, unfortunately, the interlayer magnetic exchange shows antiferromagnetic (AFM) coupling with zero net magnetic moments. Even though antiferromagnetic spintronics have been proven to be useful in recent years,[29] manipulating their interlayer coupling between FM and AFM is still desired for the sake of easy read/write in spintronics.

Here, we perform first-principles density functional theory (DFT) calculations and propose an effective way to transit interlayer AFM 2H-VX_2 (X = S and Se) bilayer to FM interlayer coupling. By calculating different magnetic coupling orders, we show that the VX_2 bilayer would prefer ferromagnetic coupling once intercalated by large sized alkali metals (AMs) with a high concentration. Note that metal intercalation into different 2D material layers has brought multiple fascinating features both experimentally and theoretically. For example, when a layer of Li/Na/K/Ca is intercalated into graphene layers (graphite), it serves as a good electrode material and a superconductor as well.[30–33] When 4d/5d transition metals intercalate into the graphene bilayer (or B-doped graphene bilayer), the system could possess an interesting topological crystalline insulating feature.[34] The intercalation of AMs into MoS_2 can trigger its phase transformation from the semiconducting 2H phase to the topological insulating 1T′ structure.[35] Experimentally, Brauer et al. have successfully intercalated some AMs in bulk VSe_2,[36] where they find that alkali metals are not simply donating electrons since the rigid band model is inadequate to match their experiments and self-consistent linear augmented planewave calculations. Later, Reshak and Auluck performed linear augmented planewave calculations on AMs intercalating layered VSe_2 and observed hybridization between AM-s,p states with V-d and Se-p orbitals, consistent with the previous argument.[37] Unfortunately, in these studies, they performed spin-unpolarized calculations on bulk materials.

Based on these results, intercalation of AMs into the 2D VX_2 *bilayer* is realistic experimentally.[35] We find that large AM intercalation could enhance the hybridization between the AM-s and V-d orbitals, which boosts super-exchange interactions between the AM and VX_2. Then, the AM layer could become spin polarized due to magnetic proximity effects. The AM-s orbital serves as a "ligand" to bridge the VX_2 layers, and the system favors FM interlayer coupling. The magnetic exchange energy can be as large as ~100 meV per unit cell, which is observable experimentally.

THEORETICAL METHODOLOGY

We use spin-polarized DFT with projector augmented wave (PAW) scheme pseudopotential[38] in the form of Perdew–Burke–Ernzerhof (PBE) type generalized gradient approximation[39] (GGA), as implemented in the Quantum–Espresso (QE) code.[40,41] The planewave basis set is used to expand the valence electrons with a cutoff energy of 80 Ry. In order to eliminate the imaging layer interactions under the three-dimensional periodic boundary condition, a vacuum space of 15 Å is added in the z-direction. The electronic and magnetic properties of two VX_2 (X = S, Se) layers with and without AM (AM = Li, Na, K, and Rb) intercalation are calculated. To incorporate the strong correlation of V-d orbitals, GGA + U is applied with the U value taken to be 3 eV. We have also tested different U values, and qualitatively consistent results

can be obtained, confirming the reliability of our selection. The reciprocal space is represented by a (12 × 12 × 1) Monkhorst–Pack k-mesh grid.[42–44] The energy and force convergences are set to be 1 × 10^{-5} eV and 0.02 eV/Å, respectively. The long-range van der Waals corrections with Grimme's DFT-D2 method is also applied.[45] Various stacking configurations and intercalation sites have been calculated, to guarantee the energetically lowest ground state.

RESULTS AND DISCUSSION

We focus our calculations on the 2H phase of VS_2 and VSe_2, which are experimentally fabricated and proved to be ferromagnetic in their monolayer form. Note that even though Nb and Ta based dichalcogenide monolayers usually show fruitful and promising charge density wave configurations, previous studies have suggested that 2H-VS_2[46] and 2H-VSe_2[47] monolayers are both dynamically stable once the spin density wave effect is accounted. This phase is also widely adopted in theoretical calculations.[22,48–50] For the VSe_2 monolayer, the 2H phase is not experimentally seen yet, so we also briefly discuss its 1T phase to verify our scheme.[10]

We find that when two layers of VX_2 (space group P-3m1) are stacked together (Fig. 1), they leave a van der Waals gap of ~3.7 Å (measured to be the nearest vertical distance between S–S and Se–Se in different layers). Our calculations show that the intralayer magnetic coupling of spin-polarized V atoms is FM, while the interlayer coupling prefers AFM (which is energetically lower than the FM coupling by 2 meV and 5 meV per supercell, corresponding to 0.2 μJ/cm^2 and 0.4 μJ/cm^2 for VS_2 and VSe_2 bilayers, respectively). Note that the stacking pattern strongly affects the interlayer magnetic coupling in the famous 2D CrI_3 bilayer.[12] However, in the current case, we find that the interlayer AFM coupling is robust against different stacking patterns. Therefore, it is intriguing to investigate and explore an effective strategy to manipulate interlayer magnetic coupling, from AFM to FM, for further magnetic storage usage. To achieve this, motivated by the experimental advancements in intercalating metal atoms in van der Waals multilayers, we propose a full AM intercalation scheme. Different intercalation geometries are investigated, and the optimal geometric structure of VX_2–AM–VX_2 (X = S, Se and AM = Li, Na, K, Rb) is shown in Fig. 1(b). We find that the AMs like to reside at the hollow site of the X-triangles and form a vertical V–AM–V line along the z-direction. Optimized geometric parameters are summarized in Table I. Upon intercalation, the VX_2 bilayer lattice expands from ~4% to 7% (compared to the non-intercalation systems) and the layer distance is also slightly increased (except for Li intercalation which reduces the interlayer distance between VX_2 due to strong attraction between Li and VX_2).

To evaluate the thermodynamic stability of such intercalation, we calculate the formation energy according to

$$E_f = E_{VX_2-AM-VX_2} - E_{VX_2-VX_2} - E_{AM},$$

where $E_{VX_2-AM-VX_2}$ and $E_{VX_2-VX_2}$ are the cohesive energies of VX_2–AM–VX_2 and VX_2–VX_2 bilayers, respectively. Chemical potential E_{AM} is taken from the cohesive energy of the bulk AM crystals. The results are listed in Table I. Note that the negative values of the formation energy suggest that such intercalation processes are
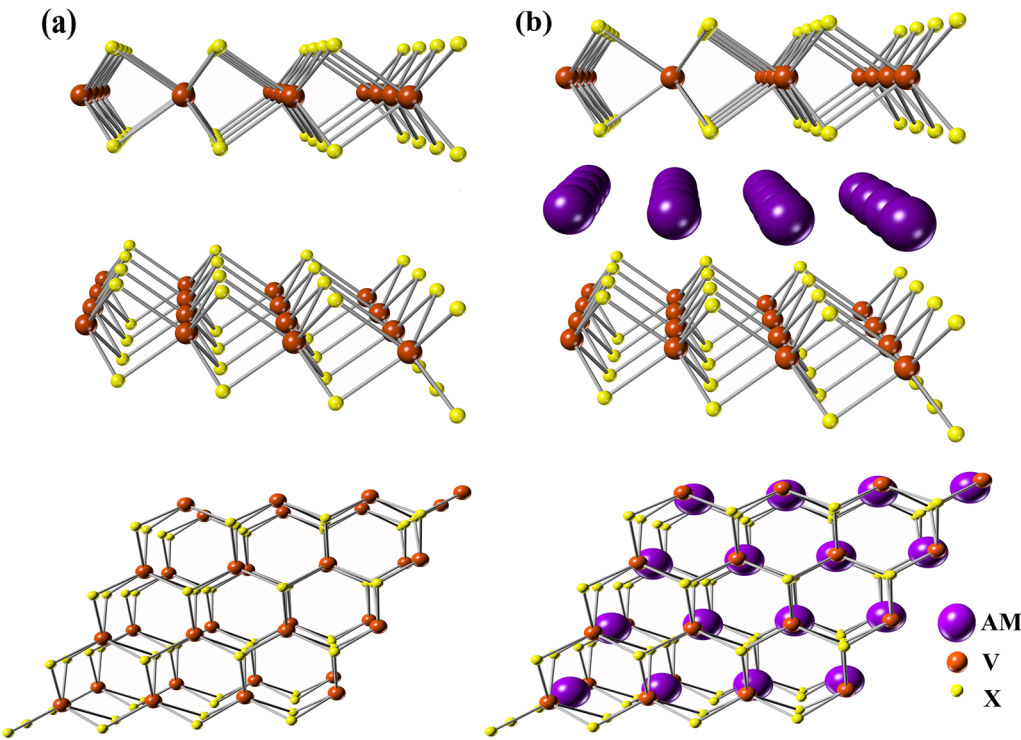
FIG. 1. The atomic structure of VX_2 bilayers (a) without AM and (b) with AM intercalation.

all exothermic, which guarantees the thermodynamic stability of the systems.

Our calculations confirm that the intralayer magnetic coupling under AM intercalation remains strong and robust and FM. We then calculate the *interlayer* magnetic exchange energy $E_{ex} = E_{AFM} - E_{FM}$ (E_{FM} and E_{AFM} are total energies of FM and AFM interlayer

TABLE I. The optimized lattice constant, distance between V and AM, formation energy, and the absolute value of magnetic moments (local magnetic moments on the V and X atoms, integrated within their own Wigner–Seitz radii) of VX_2 without and with AM intercalation. In each layer, the magnetic moments of V and X are in opposite spin channels.

	Lattice constant (Å)	V–AM (Å)	E_f (eV/f.u.)	$|m_V|$ (μ_B)	$|m_X|$ (μ_B)
VS_2–VS_2	3.20	. . .	. . .	1.50	0.26
VS_2–Li–VS_2	3.33	3.27	−2.30	2.07	0.29
VS_2–Na–VS_2	3.37	3.56	−2.10	2.08	0.30
VS_2–K–VS_2	3.40	3.88	−1.86	2.10	0.32
VS_2–Rb–VS_2	3.42	4.02	−1.77	2.12	0.33
VSe_2–VSe_2	3.36	. . .	. . .	1.75	0.38
VSe_2–Li–VSe_2	3.49	3.45	−2.24	2.32	0.41
VSe_2–Na–VSe_2	3.53	3.75	−2.13	2.33	0.42
VSe_2–K–VSe_2	3.58	4.08	−1.92	2.34	0.42
VSe_2–Rb–VSe_2	3.58	4.21	−2.01	2.38	0.50

couplings, respectively), with its positive (negative) value representing the FM (AFM) ground state. The results are shown in Fig. 2(a). One observes a strong size effect on the exchange energy. In the case of the VS_2 bilayer, under Li intercalation, the E_{ex} remains to be −2 meV (per supercell). However, when one introduces larger AMs, they serve as a magnetic "bridge" and the two VS_2 layers prefer FM coupling, with the largest E_{ex} of 15 meV (Rb intercalation). Such a size effect becomes stronger in the VSe_2 bilayer system. We find that E_{ex} is −62.17 meV and −33.81 meV for VSe_2–Li–VSe_2 and VSe_2–Na–VSe_2, respectively, while it drastically increases to positive values of 7 meV and 97 meV in VSe_2–K–VSe_2 and VSe_2–Rb–VSe_2 respectively.

We also performed similar calculations on the 1T-VSe_2 system, as stated previously. We find that without AM intercalation, the interlayer magnetic exchange energy is −2 meV. After intercalating a K layer and a Rb layer, it drastically increases its value to 406 meV and 424 meV, respectively (other AM intercalation does not flip the AFM feature to FM coupling).

The magnetic exchange variation under AM intercalation can be understood as a result of two competing magnetic coupling mechanisms [Fig. 2(b)]. Each V atom is in its +4 oxidation state, leaving only one d orbital unpaired, which occupies a single degenerated d_z^2 orbital. This is consistent with our calculations that each VX_2 unit contributes ~1 μ_B magnetic moment. Therefore, the direct exchange between the two layers results in AFM coupling. This magnetic coupling is schematically plotted in the left panel of Fig. 2(b). Once a layer of AM is introduced, owing to magnetic proximity effects, the
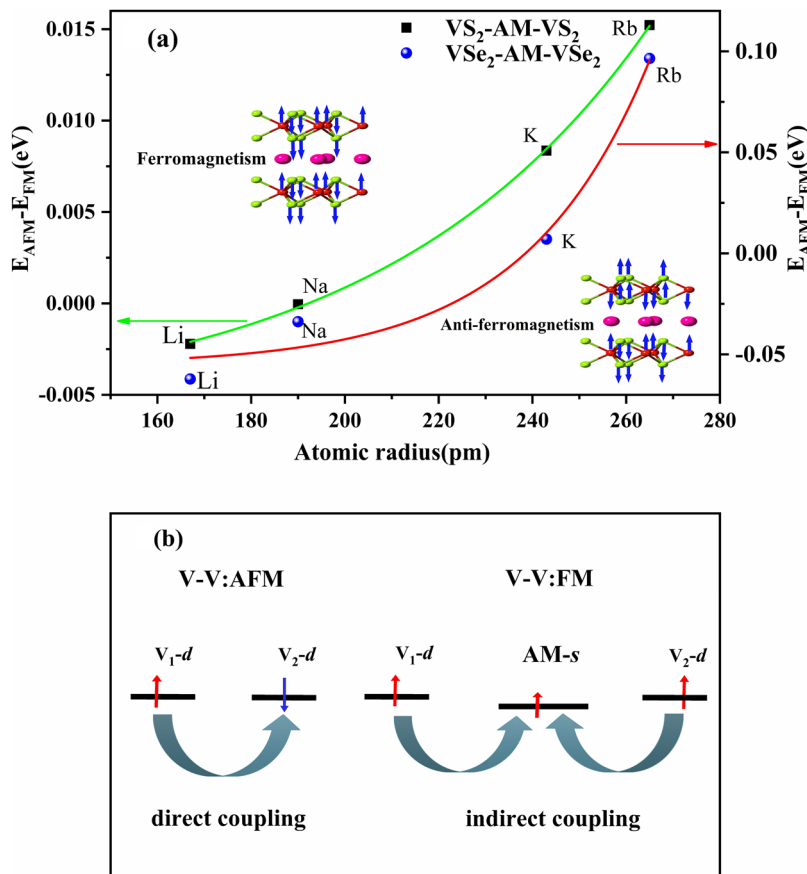
FIG. 2. (a) The variation of exchange energy with respect to intercalation atomic radius. The solid lines are fitting results. (b) Schematic plot of direct (left panel) and indirect (right panel) magnetic exchange mechanisms.

AM can be slightly magnetized, even though they are s-orbital based elements and the orbitals are itinerant. Hence, the magnetic coupling between the V-d_z^2 and the itinerant s-orbital emerges[51] [Ruderman-Kittel-Kasuya-Yosida (RKKY) picture]. Therefore, another competing magnetic exchange mechanism is an indirect super exchange between the two VX_2 layers. No matter parallel or antiparallel coupling is favored between d and s orbitals, the two VX_2 layers always prefer FM coupling. This is shown in the right panel of Fig. 2(b). When the large size AM is used, the indirect coupling dominates, and FM coupling becomes more stable than the AFM coupling. This is consistent with the carrier modulating magnetic exchange in organo-metallic frameworks.[52] Our calculations reveal that the local magnetic moment on each AM is in the range of 0.001–0.01 μ_B.

We examine their electronic properties by calculating band dispersions and projected density of states (PDOS) (Fig. 3). Since the results of AFM VX_2–AM–VX2 are similar, and those of FM systems are similar, we only take one example of each case to illustrate these results. Without any intercalations [Fig. 3(a)], the AFM VX_2 bilayer shows a semiconducting feature (bandgaps of VS$_2$ and VSe$_2$ bilayer are 0.72 eV and 0.75 eV, respectively). Both valence band maximum (VBM) and conduction band minimum (CBM) lie at the K-point (1/3, 1/3, 0). This is consistent with the honeycomb lattice with a staggered on-site potential energy on V and the X_2 moiety (sublattice-A and B). This suggests that the bilayer VX_2 can

serve as potential valleytronic devices for future information storage, similar to 2H-MoS$_2$, once the multiplication of inversion ($\mathcal{P}$) and time-reversal ($\mathcal{T}$) symmetry are broken[53,54] (such as by applying a gate voltage). When a small sized AM layer is introduced, it mainly serves as highly n-type dopant to the system. We perform Bader's charge analysis method[55,56] to analyze the charge transfer after AM intercalation. Bader's charge analysis scheme is based on the total electron density distribution in the real space, which avoids the artificial atomic orbital assignment as in the Mulliken or Hirshfeld schemes (which is also not a straightforward approach for the planewave basis set). It divides the electrons onto different nuclei according to the zero flux surfaces surrounding them, which is defined as the electron density minimum distribution perpendicular to the surface. The Bader's charge analysis scheme is widely used to analyze electron redistributions from periodic crystals to zero-dimensional molecules.[57–59] For example, we show that about 0.6 (or 0.8) electrons are transferred from a Li atom to the VSe$_2$ (or VS$_2$) bilayer.[60] As shown in Fig. 3(b), the conduction band is moved down below the Fermi level. The bandgap between the VBM and CBM is also slightly reduced. For example, in VS$_2$–Li–VS$_2$, the VBM and CBM locate at −1.733 and −1.124 eV (relative to Fermi), respectively, leaving a small bandgap of 0.05 eV. In addition, the AM layer is not magnetized (local magnetic moment of 0 μ_B). From the PDOS results, we see that a small overlap (about
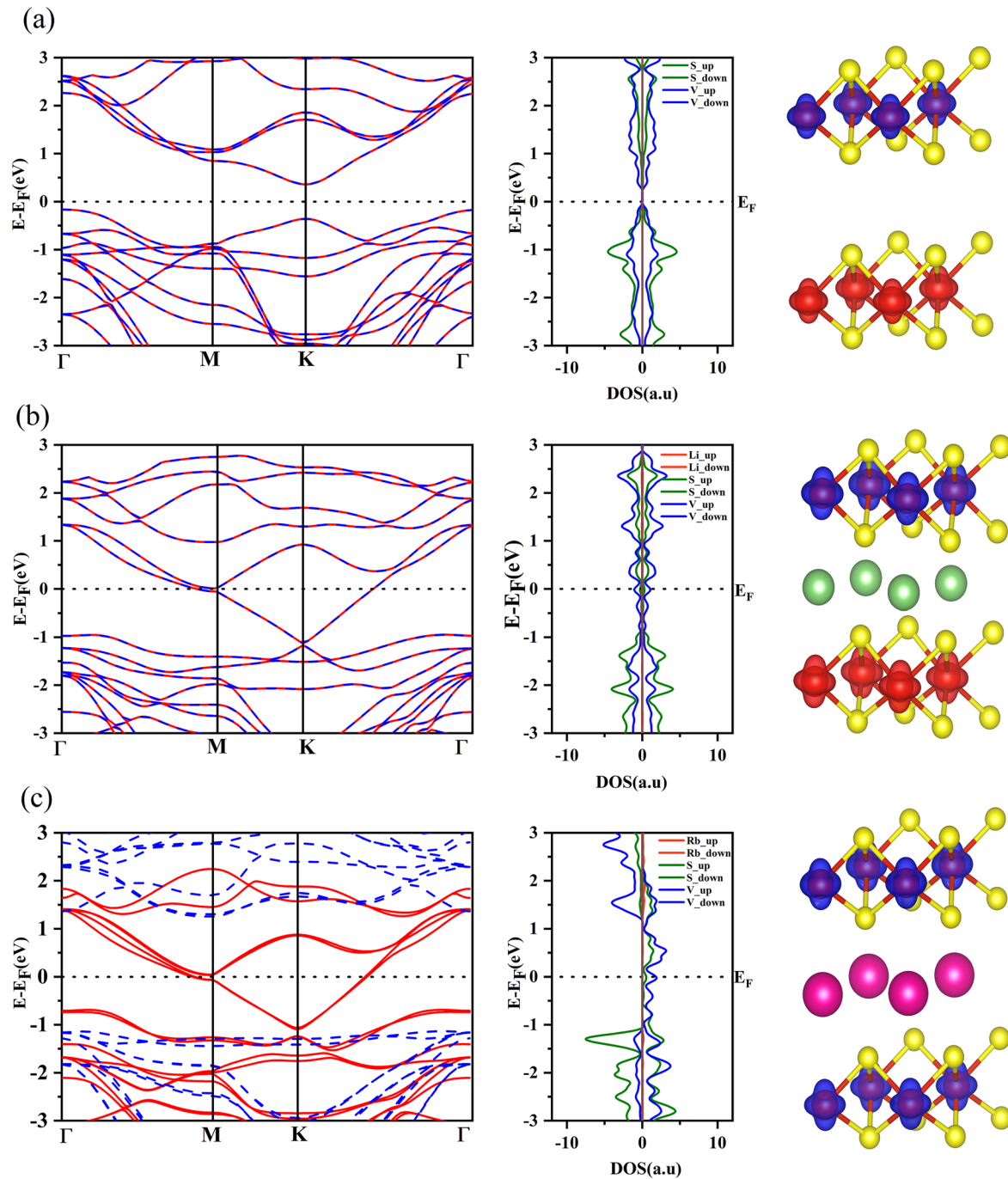
FIG. 3. Calculated band structure, PDOS, and spin density (isosurface value of 0.25 electrons/Å^3) of (a) AFM VS_2–VS_2, (b) AFM VS_2–Li–VS_2, and (c) FM VS_2–Rb–VS_2. Solid (red) and dashed (blue) lines correspond to the majority and minority spin channels, respectively.

2 eV below the Fermi level) occurs between the Li-s and S-p_z orbitals. It slightly enlarges the energy dispersion of honeycomb VX_2 lattice band dispersion. We assign that this is the reason for narrowing down of the bandgap. Hence, two interaction mechanisms occur

after Li intercalation. One is the Li electron transfer, forming a Li^+ and n-doped VX_2. The other is weak hybridization between the Li-s and X-p orbitals, which slightly modifies the band dispersion. We note that the PDOS and band dispersion results suggest that the

former ionic feature dominates the binding interaction, while the latter covalent feature interaction is much weaker (as it is deeply below the Fermi level), consistent with reversible intercalations observed in electrochemical experiments.[61] As the size of the AM layer becomes larger (e.g., VS_2–Rb–VS_2), the AM is magnetized (0.001 μ_B per Rb) owing to proximity effects. The indirect exchange makes the whole system prefer FM coupling, so that the spin-up and spin-down channel splits energetically [Fig. 3(c)]. The weak Rb-s and S-p_z orbital hybridization still exists. We can see that the spin-up channel is highly conductive, while the spin-down channel opens a wide bandgap of 2.59 eV around the Fermi level, showing a semiconducting character. Thus, this FM sandwich structure is a good half-metal, showing a 100% spin filtering effect. In this regard, we suggest that AM intercalation can effectively modulate the VX_2 bilayer from AFM semiconducting to AFM metallic and then to FM half-metallic behavior.

CONCLUSION

In conclusion, we have performed first-principles spin-polarized DFT calculations and predict an effective strategy to trigger a magnetic exchange coupling transition from AFM to FM between the two VX_2 layers. We show that once intercalating a layer of alkali metals, the competing direct and indirect exchange mechanisms can tune the total magnetic exchange energy, depending on the size of alkali metals. With K and Rb intercalation, the VX_2 bilayer prefers an FM coupling (owing to indirect RKKY mechanism), with its exchange energy observable under low temperature. The system exhibits a widely tunable electronic property, from AFM semiconducting to AFM metallic and then to FM half-metallic conductivity. Such itinerant indirect exchange mechanism can be applied to other AFM systems to effectively tune their magnetic coupling properties. Due to the experimental advances to intercalate and extract Li (and other alkali metals) in between van der Waals layer compounds (such as in Li-ion batteries), one can use this electrochemical technology to control magnetic moments and other properties (such as magneto-optic responses) via external electrochemical approaches.

ACKNOWLEDGMENTS

The data that support the findings of this study are available from the corresponding author upon reasonable request.

REFERENCES

[1] J. Li, Y. Ding, W. Zhang, and P. Zhou, Acta Phys.-Chim. Sin. **35**, 1058–1077 (2019).
[2] E. V. Castro, K. Novoselov, S. Morozov, N. Peres, J. L. Dos Santos, J. Nilsson, F. Guinea, A. Geim, and A. C. Neto, Phys. Rev. Lett. **99**, 216802 (2007).
[3] J. L. Dos Santos, N. Peres, and A. C. Neto, Phys. Rev. Lett. **99**, 256802 (2007).
[4] I. Gierz, T. Suzuki, R. T. Weitz, D. S. Lee, B. Krauss, C. Riedl, U. Starke, H. Höchst, J. H. Smet, and C. R. Ast, Phys. Rev. B **81**, 235408 (2010).

[5] B. Huang, G. Clark, E. Navarro-Moratalla, D. R. Klein, R. Cheng, K. L. Seyler, D. Zhong, E. Schmidgall, M. A. McGuire, and D. H. Cobden, Nature **546**, 270 (2017).
[6] S. Jiang, L. Li, Z. Wang, K. F. Mak, and J. Shan, Nat. Nanotechnol **13**, 549 (2018).
[7] K. L. Seyler, D. Zhong, D. R. Klein, S. Gao, X. Zhang, B. Huang, E. Navarro-Moratalla, L. Yang, D. H. Cobden, and M. A. McGuire, Nat. Phys. **14**, 277 (2018).
[8] C. Huang, Y. Du, H. Wu, H. Xiang, K. Deng, and E. Kan, Phys. Rev. Lett. **120**, 147601 (2018).
[9] C. Gong, L. Li, Z. Li, H. Ji, A. Stern, Y. Xia, T. Cao, W. Bao, C. Wang, and Y. Wang, Nature **546**, 265 (2017).
[10] M. Bonilla, S. Kolekar, Y. Ma, H. C. Diaz, V. Kalappattil, R. Das, T. Eggers, H. R. Gutierrez, M.-H. Phan, and M. Batzill, Nat. Nanotechnol. **13**, 289 (2018).
[11] K. Xu, P. Chen, X. Li, C. Wu, Y. Guo, J. Zhao, X. Wu, and Y. Xie, Angew. Chem., Int. Ed. **52**, 10477–10481 (2013).
[12] N. Sivadas, S. Okamoto, X. Xu, C. J. Fennie, and D. Xiao, Nat. Lett. **18**, 7658–7664 (2018).
[13] S. Jiang, J. Shan, and K. F. Mak, Nat. Mater. **17**, 406 (2018).
[14] M. Chhowalla, H. S. Shin, G. Eda, L.-J. Li, K. P. Loh, and H. Zhang, Nat. Chem. **5**, 263 (2013).
[15] J. Feng, X. Sun, C. Wu, L. Peng, C. Lin, S. Hu, J. Yang, and Y. Xie, J. Am. Chem. Soc. **133**, 17832–17838 (2011).
[16] Y. Ding, Y. Wang, J. Ni, L. Shi, S. Shi, and W. Tang, Physica B **406**, 2254–2260 (2011).
[17] W. Feng, Y. Yao, W. Zhu, J. Zhou, W. Yao, and D. Xiao, Phys. Rev. B **86**, 165108 (2012).
[18] D. Gao, Q. Xue, X. Mao, W. Wang, Q. Xu, and D. Xue, J. Mater. Chem. C **1**, 5909–5916 (2013).
[19] Y. Jing, Z. Zhou, C. R. Cabrera, and Z. Chen, J. Phys. Chem. C **117**, 25409–25413 (2013).
[20] D. W. Murphy, C. Cros, F. J. Di Salvo, and J. Waszczak, Inorg. Chem. **16**, 3027–3031 (1977).
[21] H. Pan, J. Phys. Chem. C **118**, 13248–13253 (2014).
[22] H. Zhang, L.-M. Liu, and W.-M. Lau, J. Mater. Chem. A **1**, 10821–10828 (2013).
[23] Y. Ma, Y. Dai, M. Guo, C. Niu, Y. Zhu, and B. Huang, ACS Nano **6**, 1695–1701 (2012).
[24] W.-Y. Tong, S.-J. Gong, X. Wan, and C.-G. Duan, Nat. Commun. **7**, 13612 (2016).
[25] J. Qi, X. Li, Q. Niu, and J. Feng, Phys. Rev. B **92**, 121403 (2015).
[26] Q. Zhang, S. A. Yang, W. Mi, Y. Cheng, and U. Schwingenschlögl, Adv. Mater. **28**, 959–966 (2016).
[27] J. Zhou and P. Jena, J. Phys. Chem. Lett. **8**, 5764–5770 (2017).
[28] G. Wiegers, Physica B+ C **99**, 151–165 (1980).
[29] V. Baltz, A. Manchon, M. Tsoi, T. Moriyama, T. Ono, and Y. Tserkovnyak, Rev. Mod. Phys. **90**, 015005 (2018).
[30] G. Profeta, M. Calandra, and F. Mauri, Nat. Phys. **8**, 131 (2012).
[31] J. Zhou, Q. Sun, Q. Wang, and P. Jena, Phys. Rev. B **90**, 205427 (2014).
[32] B. Ludbrook, G. Levy, P. Nigge, M. Zonno, M. Schneider, D. Dvorak, C. Veenstra, S. Zhdanovich, D. Wong, and P. Dosanjh, Proc. Natl. Acad. Sci. U. S. A. **112**, 11795–11799 (2015).
[33] J. Lu, Z. Chen, F. Pan, Y. Cui, and K. Amine, Electrochem. Energy Rev. **1**, 35–53 (2018).
[34] J. Zhou and P. Jena, Phys. Rev. B **95**, 081102 (2017).
[35] M. Kan, J. Wang, X. Li, S. Zhang, Y. Li, Y. Kawazoe, Q. Sun, and P. Jena, J. Phys. Chem. C **118**, 1515–1522 (2014).
[36] H. Brauer, H. Starnberg, L. Holleboom, V. Strocov, and H. Hughes, Phys. Rev. B **58**, 10031 (1998).
[37] A. H. Reshak and S. Auluck, Physica B **349**, 310–315 (2004).
[38] P. E. Blöchl, Phys. Rev. B **50**, 17953 (1994).
[39] J. P. Perdew, K. Burke, and M. Ernzerhof, Phys. Rev. Lett. **77**, 3865 (1996).

[40] P. Giannozzi, O. Andreussi, T. Brumme, O. Bunau, M. Buongiorno Nardelli, M. Calandra, R. Car, C. Cavazzoni, D. Ceresoli, and M. Cococcioni, J. Phys.: Condens. Matter **29**, 465901 (2017).

[41] P. Giannozzi, S. Baroni, N. Bonini, M. Calandra, R. Car, C. Cavazzoni, D. Ceresoli, G. L. Chiarotti, M. Cococcioni, and I. Dabo, J. Phys.: Condens. Matter **21**, 395502 (2009).

[42] H. J. Monkhorst and J. D. Pack, Phys. Rev. B **13**, 5188 (1976).

[43] E. Davidson, in *Methods in Computational Molecular Physics* (Plenum New York, City, 1983), Vol. 113, p. 95.

[44] M. Methfessel and A. Paxton, Phys. Rev. B **40**, 3616 (1989).

[45] S. Grimme J. Comput. Chem. **27**, 1787–1799 (2006).

[46] E. B. Isaacs and C. A. Marianetti, Phys. Rev. B **94**, 035120 (2016).

[47] M. Esters, R. G. Hennig, and D. C. Johnson, Phys. Rev. B **96**, 235147 (2017).

[48] H. L. Zhuang and R. G. Hennig, Phys. Rev. B **93**, 054429 (2016).

[49] N. Luo, C. Si, and W. Duan, Phys. Rev. B **95**, 205432 (2017).

[50] C. S. Rout, B.-H. Kim, X. Xu, J. Yang, H. Y. Jeong, D. Odkhuu, N. Park, J. Cho, and H. S. Shin, J. Am. Chem. Soc. **135**, 8720–8725 (2013).

[51] T. Dietl, A. Haury, and Y. Merle d'Aubigné, Phys. Rev. B **55**, R3347 (1997).

[52] J. Zhou and Q. Sun, Nanoscale **6**, 328–333 (2014).

[53] D. Xiao, G.-B. Liu, W. Feng, X. Xu, and W. Yao, Phys. Rev. Lett. **108**, 196802 (2012).

[54] Q. H. Wang, K. Kalantar-Zadeh, A. Kis, J. N. Coleman, and M. S. Strano, Nat. Nanotechnol. **7**, 699 (2012).

[55] G. Henkelman, A. Arnaldsson, and H. Jónsson, Comput. Mater. Sci. **36**, 354–360 (2006).

[56] E. Sanville, S. D. Kenny, R. Smith, and G. Henkelman, J. Comput. Chem. **28**, 899–908 (2007).

[57] J. Zhou, S. Giri, and P. Jena, Phys. Chem. Chem. Phys. **16**, 20241–20247 (2014).

[58] S. Zhang, J. Zhou, Q. Wang, and P. Jena, J. Phys. Chem. C **120**, 3993–3998 (2016).

[59] X. Su, A. Kushima, C. Halliday, J. Zhou, J. Li, and T. A. Hatton, Nat. Commun. **9**, 4701 (2018).

[60] W. Tang, E. Sanville, and G. Henkelman, J. Phys.: Condens. Matter **21**, 084204 (2009).

[61] M. S. Whittingham, C. Siu, and J. Ding, Acc. Chem. Res. **51**, 258–264 (2018).